coatings

MDPI

Article

Effect of Solid Sodium Silicate on Workability, Hydration and Strength of Alkali-Activated GGBS/Fly Ash Paste

Tingkai Dong [1], Tao Sun [2,3,*], Fang Xu [4], Gaoshang Ouyang [1], Hongjian Wang [5], Fan Yang [6] and Ziyan Wang [1]

1 School of Materials Science and Engineering, Wuhan University of Technology, Wuhan 430070, China
2 State Key Laboratory of Silicate Materials for Architectures, Wuhan University of Technology, Wuhan 430070, China
3 Wuhan University of Technology Advanced Engineering Technology Research Institute of Zhongshan City, Wuhan 528400, China
4 Faculty of Engineering, China University of Geosciences, Wuhan 430074, China
5 Shandong High Speed Maintenance Group Co., Ltd., Hubei Company, Wuhan 430010, China
6 China Construction Advanced Technology Institute, Wuhan 430073, China
* Correspondence: sunt@whut.edu.cn

Abstract: Based on economic and environmental considerations, the recycling economy of mineral waste has been found to have great potential and economic benefits worldwide, in which alkali-activated cementitious materials are one of the main developing directions. The alkali activators commonly used in alkali-activated cementitious materials are the composite activators of sodium silicate solution and solid sodium hydroxide, which not only need to deal with high viscosity and corrosive chemicals, but also need to be prepared in advance and properly stored. In this paper, ground granulated blast furnace slag (GGBS) and fly ash were used as precursors, while solid sodium silicate powder was applied as the alkali activator. In addition, the precursors were mixed with the activator in advance and activated by adding water to prepare alkali-activated GGBS/fly ash cement. The influence of precursor components, the dosage of the alkali activator and the liquid–solid ratio on the working performance, mechanical strength and hydration process of alkali-activated cement was studied. The results showed that the further incorporation of GGBS accelerated the alkali activation reaction rate and improved the strength of the specimen. However, in the specimen with GGBS as the main component of the precursor, the main hydration product was *C-A-S-H gel*, which was different in the structural order and quantity. The compressive strength indicated that there was the best amount of activator to match it in terms of the precursor with certain components. A too high or too low amount of activator will hinder the alkali activation reaction. This study can provide some significant reference material for the use of solid alkali activators in alkali-activated cementitious materials.

Keywords: solid powdered sodium silicate; workability; GGBS–fly ash blends; alkali activation; compressive strength

Citation: Dong, T.; Sun, T.; Xu, F.; Ouyang, G.; Wang, H.; Yang, F.; Wang, Z. Effect of Solid Sodium Silicate on Workability, Hydration and Strength of Alkali-Activated GGBS/Fly Ash Paste. *Coatings* **2023**, *13*, 696. https://doi.org/10.3390/coatings13040696

Academic Editor: Andrea Nobili

Received: 2 March 2023
Revised: 17 March 2023
Accepted: 22 March 2023
Published: 29 March 2023

1. Introduction

Concrete is an important part of modern architecture, and about 12 billion tons of concrete are produced every year [1], so we have to face the problems of energy consumption and CO_2 emissions brought about by cement production, and the continuous reduction in mineral materials as aggregates. For environmental and economic considerations, it is urgent to apply recyclable waste to the construction field. Karalar et al. [2] used waste marble powder to replace parts of cement for concrete preparation. Although the compressive strength of concrete has decreased, the replacement rate of 10~20% is feasible from the perspective of bending and cracking behavior. Qaidi et al. [3] used PET plastic waste to partially replace fine aggregate for the preparation of lightweight concrete with low conductivity and high toughness. Zeybek et al. [4] applied waste glass to concrete production and found that the compressive strength of concrete decreased when waste

glass powder was used to replace part of cement and that the appropriate replacement rate was 20%; however, when waste glass powder is used to replace a part of the cement and waste glass particles were used to replace a part of the aggregate, the mechanical strength of concrete was improved by 10% in its substitution rate. Karalar et al. [5] used coal bottom ash to replace fine aggregate to prepare reinforced concrete beams, taking the bending and fracture behavior of the beam as the performance index, in which a 75% substitution rate was the most appropriate. Qaidi et al. [6] found that the use of waste glass as an aggregate in concrete can effectively reduce the static load of concrete, although it will reduce the workability and mechanical properties of concrete. Shcherban et al. [7] used coconut fiber as the fiber reinforcement of concrete, and found that its mechanical properties and elastic modulus were improved, and the best fiber reinforcement rate was 1.75%. Beskopylny et al. [8] used rubber tree seed shell to replace a part of coarse aggregate for concrete manufacturing. When the substitution rate is between 2% and 6%, the microstructure of concrete achieved the highest density. It is estimated that this method can reduce the consumption of mineral coarse aggregate by 8%. In addition, alkali-activated cementitious materials are also an important research direction because they can partially or completely use solid waste instead of cement.

Alkali-activated cementitious materials are materials that react with alkali activators using silica–aluminum materials with pozzolanic activity or potential hydraulic properties [9,10]. According to the differences in their precursors, alkali-activated cementing material systems can be divided into two categories [11,12]. One is a calcium-rich and silica-rich system represented by GGBS, whose main reaction products are *C-A-S-H gel* with a low Ca/Si ratio and high Al inclusion. The other is an aluminum-rich and silica-rich system represented by (low calcium) fly ash, the reaction product of which is *N-A-S-H gel* with a three-dimensional network. In recent years, scholars generally believe that it is an environmentally friendly and sustainable alternative to traditional Portland cement. On one hand, because aluminum silicate precursor can partially or completely use industrial wastes, and the production process of alkali-activated cementing materials does not require 'two grindings and one burning' [13], it solves the three major problems that commonly exist in the traditional cement industry: high energy consumption, difficulty supplying raw materials and large carbon dioxide emissions. On the other hand, alkali-activated cementing materials generally perform better than cement; they have a high early strength, fast hardening, chemical corrosion resistance and good durability [14,15]. At present, the most commonly used alkali activator is the composite activator of sodium silicate solution and solid sodium hydroxide. The following problems need to be faced during the application: (1) in the configuration of sodium silicate solution, it is necessary to deal with the high viscosity of sodium silicate solution and caustic sodium hydroxide; (2) the sodium silicate solution needs to be pre-configured and needs a certain standing time after the configuration is completed; (3) the storage and handling of the chemical solution have to be faced. In contrast, it is more convenient and safer to mix the solid activator with the precursor in advance, and add water to activate it during application [16,17]. Meanwhile, research on the application of solid base activators is relatively lacking at present.

Common solid activators include strong alkali, silicate, carbonate, sulfate and aluminate, etc. [18–20]. Zhang et al. [21] used sodium hydroxide and sodium carbonate powder as composite solid activators, and the compressive strength at 28 days exceeded 50 MPa. Jiang et al. [22] used calcined sodium carbonate as the alkali activator, and found that its activation effect was similar to that of sodium silicate solution. Koloušek et al. [23] prepared alkali-activated cement by calcination of kaolin and solid sodium hydroxide, whose compressive strength was still less than 1 MPa at 7 days. Hajimohammadi et al. [24–26] mixed geothermal silica with solid sodium aluminate as a source of silica, alumina and alkali, but the slurry took 14 days to set and harden until the mold was removed. Feng et al. [27] studied the alkali-activation effect of albite mixed with sodium hydroxide or sodium carbonate powder at a high temperature, and found that its compressive strength reached 40 MPa at 28 days. Sturm et al. [28] used rice husk ash as the precursor and solid sodium aluminate

as the activator to prepare alkali-activated cement, which exhibited a compressive strength of 30.1 MPa after 7 days under the curing temperature of 80 °C. It can be found that when using non-silicates as solid activators, a higher compressive strength is usually achieved by calcination, the application of strong alkalis or higher reaction temperatures. In addition, the early strength is generally lower because the base activators do not provide additional [SiO_4] monomers. This is contrary to the original intention of developing solid activators.

When silicate is used as an alkali activator, these problems can be effectively avoided; Ma et al. [29] used three different types of solid sodium silicate powders (Na_2SiO_3-anhydrous, $Na_2SiO_3{\cdot}5H_2O$, and $Na_2SiO_3{\cdot}9H_2O$) individually as activators. Na_2SiO_3-anhydrous had the most significant alkali activation effect in terms of compressive strength. Liu et al. [30] used sodium silicate powder as the alkali activator, and the strength of the alkali-activated cement after 28 days reached 20.5 MPa when the modulus was 0.5. Yang et al. [31] used the compound alkali activator of sodium silicate powder and sodium hydroxide powder, and produced a good activation effect on the precursor composed of GGBS and fly ash, with the compressive strength exceeding 50 MPa at 28 days. In addition, Temuujin [32], Nematollahi [33] and Yang [34] et al. also used GGBS and fly ash, as precursors with single Na_2SiO_3 or composite activators consisting of $Na_2SiO_3{\cdot}nH_2O$ and NaOH were considered as activators, from which alkali-activated cement with a compressive strength of 40~70 MPa at 28 days was prepared at room temperature. Their research shows that sodium silicate powder can be feasibly used as a solid alkali activator, but their research focuses on the chemical composition and microstructure of hydration products, and lacks the mechanism of the influence of sodium silicate powder on the working performance and mechanical strength of alkali-activated cement.

In this paper, low-calcium fly ash and GGBS were used as precursors, and sodium silicate powder with modulus of 2.0 was used as the solid alkali activator. The mechanisms of the precursor components, the sodium silicate content and the liquid–solid ratio on the working and mechanical properties of alkali-activated cement were investigated. The type and microstructure of the hydration products were characterized by XRD, TG/DTG and FTIR.

2. Experimental Program

2.1. Materials

The ground granulated blast furnace slag (GGBS) used in this study's test was obtained from Wuhan Iron and Steel Group Co., Ltd (Wuhan, China). According to the national standard GB/T 203, the reactivity of the GGBS is evaluated by the quality factor (K), is determined by the total amount of oxides (CaO, Al_2O_3, and MgO), and is divided by total amount of oxides (SiO_2, MnO, and TiO_2), as shown in Equation (1); in this paper, the quality factor K value is 1.6. The F grade fly ash was obtained from Zhuhai Power Plant Co., Ltd (Zhuhai, China). The solid alkali activator was an instant powdered sodium silicate with a modulus of 2.0, purchased from Henan Platinum New Materials Co., Ltd (Hennan, China), which is a kind of white powder material that can be rapidly dissolved in water, and whose aqueous solution is alkaline. The chemical compositions of the cementitious materials are shown in Table 1, where ω means the mass fraction of oxides (wt.%). LOI in the table is the abbreviation for loss on ignition, which refers to the percentage of the mass loss of raw materials that have lost external moisture after drying in the temperature range of 105~110 °C and burning for a long time under certain high-temperature conditions.

$$K = \frac{\omega_{CaO} + \omega_{MgO} + \omega_{Al_2O_3}}{\omega_{SiO_2} + \omega_{MnO} + \omega_{TiO_2}} \quad (1)$$

The cumulative particle size distribution of GGBS and fly ash is shown in Figure 1; the mean particle sizes (D50) of the GGBS and fly ash are 12.1 and 16.5 μm, and their specific surface areas are 1.13 m^2/g and 1.11 m^2/g, respectively.

Table 1. Chemical composition of cementitious materials (wt.%).

Material	SiO_2	Al_2O_3	CaO	MgO	SO_3	Fe_2O_3	MnO	TiO_2	LOI
GGBS	30.6	15.5	36.7	8.9	2.6	1.1	0.5	1.0	1.1
Fly ash	48.2	33.1	5.1	1.2	1.0	5.0	0.1	0.9	2.8

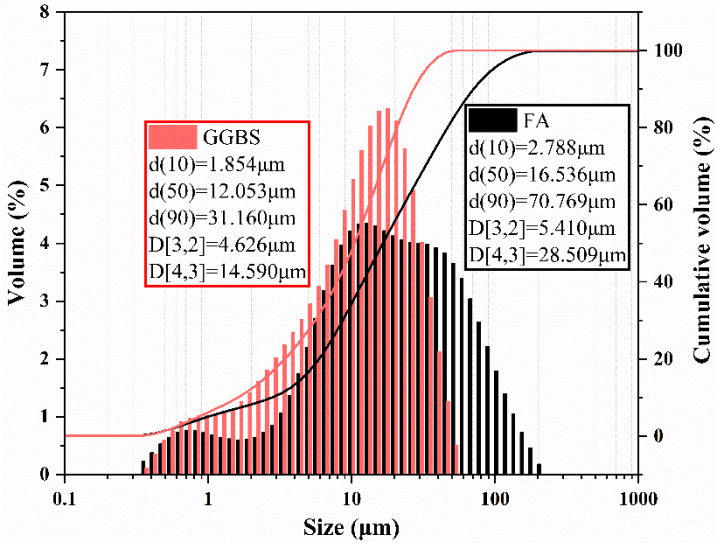

Figure 1. Particle size distribution of cementitious material.

The crystal phase diagram of the GGBS and fly ash is shown in Figure 2. It can be seen that the GGBS has no obvious crystalline phase, and the peak hump between 25° and 35° indicates that the GGBS contains a large number of amorphous phases. Meanwhile, the main crystalline phases of the fly ash are quartz, mullite and hematite, and the fly ash also contains some amorphous phases, with the peak hump between 17° and 35°, which means that both the GGBS and the fly ash have partial cementing and pozzolanic properties. The location difference of the amorphous peak hump represents the structural difference between the GGBS and fly ash.

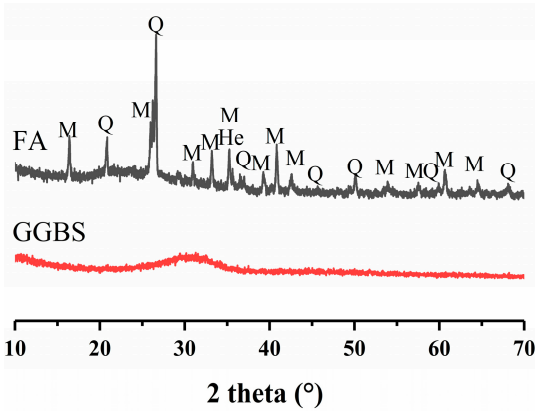

Figure 2. XRD patterns of precursors. Legend: Q = quartz; M = mullite; He = hematite.

2.2. Mix Proportion Design and Slurry Preparation

2.2.1. Mixture Proportions

The precursor mass of the group of specimens molded in this study was 350 g. The three experimental variables were the components of the precursor (P), the dosage of the solid sodium silicate powder (S), and the liquid–solid ratio (L), in which the liquid–solid ratio is water/(precursor + powdered sodium silicate). The specific mix ratio is shown in Table 2.

Table 2. Mix proportions of GGBS/fly ash pastes.

Specimen	Fly Ash	GGBS	Activator	Water
P14	280.0	70.0	80.0	98.9
P23	210.0	140.0		
P32	140.0	210.0		
P41	70.0	280.0		
S50	70.0	280.0	50.0	92.0
S60			60.0	94.3
S70			70.0	96.0
S90			90.0	101.2
S100			100.0	103.5
S110			110.0	105.8
L0.20	70.0	280.0	80.0	86.0
L0.26				111.8
L0.30				129.0
L0.32				137.6
L0.35				150.5
L0.38				163.4

Note: The unit is g, the letters P, S and L in the sample number represent the mass ratio of GGBS/fly ash in the precursor component, the mass of solid sodium silicate powder, and the liquid–solid ratio, respectively. It should be noted that groups P41, S80 and L0.23 are the same group of test pieces.

When preparing the specimen, we weighed the fly ash, GGBS and powdered sodium silicate according to Table 2, placed them in the clear slurry mixing pot and stirred them evenly after adding water of the corresponding quality; we stirred them (according to GB/T7671-1999) at low speed for 120 s, stopped for 15 s, and then stirred them quickly for 120 s. Finally, the slurry was loaded into the molds with a dimension of 40 mm × 40 mm × 160 mm with film covered. It was placed in the standard curing chamber with a temperature of (20 ± 2) °C and relative humidity (≥95%) for 24 h until the specified age and demolded after 24 h.

2.2.2. Testing Methods

1. Working performance, setting time and mechanical properties

A slump flow test was used to evaluate the working performance of the slurry based on GB/T 8077-2012; after filling the fluidity mold with the newly mixed slurry to be measured, the mold was quickly lifted from the glass plate in the vertical direction. After 30 s, the average of the two maximum diameters in the vertical direction of each other was taken as the fluidity.

The setting time of the slurry was determined according to GB/T 1346-2011.

The 40 mm × 40 mm × 160 mm samples were adopted to measure the compressive strength based on GB/T 17671-1999. The compressive strength is given by Equation (2), as follows:

$$f_c = \frac{F}{A_c} \tag{2}$$

where f_c is the compressive strength (MPa), F is the maximum load at failure (N), and A_c is the cross-sectional area of the specimen on which the compressive force acts (mm^2).

2. Mineralogical compositions and microstructure

The mineralogical compositions of the specimens were monitored using X-ray diffraction (XRD) with a Bruker D8 Advanced X-ray diffractometer (Bruker Corporation, Billerica, MA, USA); the Fourier Transform infrared spectroscopy (FTIR) measurement was performed in a Nicolet 6700 instrument (Thermo Fisher Scientific, Massachusetts, USA) with the wave numbers ranging from 4000 to 600 cm^{-1}.

A thermogravimetry (TG) analysis was conducted in an STA449F3 instrument (NETZSCH, Free State of Bavaria, Germany); the grinded powder samples were heated from 40

to 1000 °C, at 10 °C/min, with nitrogen as the carrier gas. All the sample analyses were carried out at the age of 7 days.

The preparation and test process are shown in Figure 3.

Figure 3. Flow chart for experiments.

3. Results and Discussion

3.1. Workability

The fluidity of each group of alkali-activated GGBS/fly ash cement is shown in Figure 4, and the setting time is shown in Figure 5. Groups P14~P41 regulated the mass ratio of GGBS/fly ash in the precursor, and the two numbers after the letter P represent the proportion of GGBS and fly ash in the precursor. On the whole, with the increase in the proportion of GGBS in the precursor, the loss of slurry fluidity is obvious, and the setting time is shortened; the reasons for this phenomenon are as follows: (1) compared with the rough particles and angular structure of GGBS, the smooth spherical particles of fly ash can play the role of a "ball bearing", reducing the loss of fluidity [35,36]; and (2) due to the high degree of polymerization and low amorphous properties of fly ash, the hydration activity of fly ash is lower than that of GGBS. With the increase in the proportion of GGBS, the active CaO in the system increases significantly, which further leads to an increase in Ca^{2+} ions that can participate in an alkali-activated reaction, speeding up the hydration reaction rate and shortening the setting time [37].

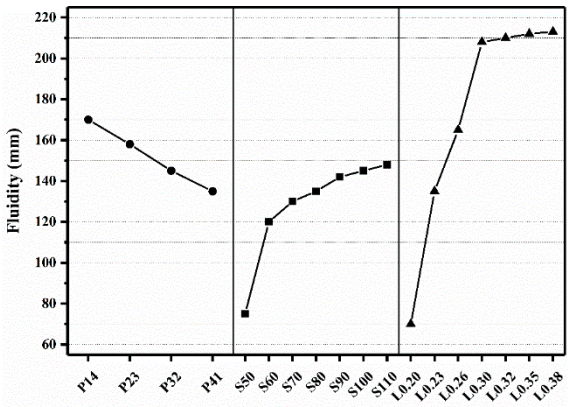

Figure 4. Effects of precursor composition, dosage of solid powdered sodium silicate and liquid–solid ratio on fluidity of fresh paste.

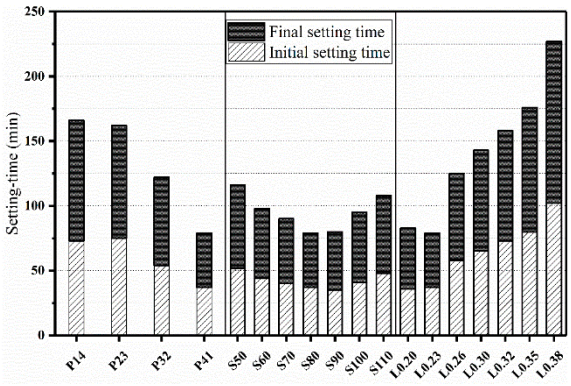

Figure 5. Effects of precursor composition, dosage of solid powdered sodium silicate and liquid–solid ratio on setting time.

When using a solid alkali activator to prepare alkali-activated cement, the process is often faced with the problem that the setting time of slurry is too long [23–26]. Therefore, subsequent studies were based on group P41, in which groups S50~S110 regulated the dosage of solid powdered sodium silicate to explore the influence of a solid alkali activator on the fluidity and setting time of alkali-activated cement; the number after the letter S represents the mass of solid powder sodium silicate. When the dosage of powdered sodium silicate in group S50 is low (50 g), the slurry almost loses its fluidity, which is only 75 mm. In group S60, a small increase in the dosage of powdered sodium silicate (10 g) will greatly improve the working performance of the slurry, reaching 120 mm. When the dosage of sodium silicate continues to increase, the rising trend seen in the fluidity of the slurry tends to be gentle. This is because when the dosage of sodium silicate is 50 g, the concentration of OH^- in the system is low, the erosion of precursor is slow, and the slurry is mainly manifested as the highly viscous sodium silicate aqueous solution and suspended particle mixture. At this point, if the content of sodium silicate is slightly increased, the concentration of OH^- is enough to erode the precursor, while if the content of sodium silicate continues to increase, excessive OH^- will form Ca $(OH)_2$ with Ca^{2+}, inhibiting an increase in the fluidity [38].

The influence of the dosage of solid powdered sodium silicate in group S on the setting time and fluidity of the slurry is not completely the same. The dosage of powdered sodium silicate in group S50 is 50 g, and the initial and final setting times are 52 and 64 min, respectively. At this time, the setting time of the slurry will be shortened with the increase in the dosage of powdered sodium silicate. The shortest setting time occurs when the dosage of powdered sodium silicate is 80 g, and when the initial and final setting times are 37 and 42 min, respectively; however, when the dosage of powdered sodium silicate continues to increase, the setting time will be prolonged. For example, when the dosage is 110 g, the initial and final setting times are 48 and 60 min, respectively. It can be seen that when the dosage of powdered sodium silicate continues to increase, the setting time of the slurry presents a trend of first shortening and then increasing; this is mainly because the alkali concentration of group S50 is too low, and the corrosion dissolution process of the precursor is slow, showing a long setting time. When the dosage of sodium silicate is increased appropriately, such as in group P41, the increase in the alkali concentration can not only improve the dissolution rate of the precursor [39], but also increase the solubility of silica and alumina in solution, which is conducive to the alkali-activated reaction [40,41]. Therefore, the setting time has been shortened to a certain extent, but the increase in the sodium silicate content makes the reaction product quickly generated and attached to the precursor particle surface so that it will hinder the dissolution process and prolong the setting time [42]. This also shows that for the precursor with certain components, the optimal dosage of the activator with fixed modulus is matched, and an activator dosage that is too high or too low will have a certain negative effect on the alkali-activated reaction.

When the mass ratio of GGBS/fly ash is 280/70 and the dosage of powdered sodium silicate is 80 g, groups L0.20~L0.38 regulate the amount of water added in order to explore the effect of the liquid–solid ratio on the setting time and fluidity of the slurry; the number after the letter L represents the specific value of the liquid–solid ratio. As a whole, the increase in the liquid–solid ratio can greatly improve the fluidity of the slurry and extend the setting time. Although water does not participate in the alkali excitation reaction, the liquid–solid ratio can affect the fluidity and setting time; because water plays a neutralization role, the increase in the amount of water will change the alkalinity of the activator (decrease the pH value) and the viscosity of the system solution (improve the fluidity), thus reducing the reaction rate and extending the setting time [43].

3.2. Mechanical Performance

The mechanical properties of groups P14~P41, S50~S110 and L0.20~L0.38 were tested, as shown in Figure 6. Among the variables discussed in this paper, the mass ratio of GGBS/fly ash has the greatest influence on the mechanical properties of the specimen. In addition, it can be observed that except for groups L0.30~L0.38, which have a high liquid–solid ratio, the strength of other groups of specimens develops rapidly, and the compressive strength at 7 days is very close to the strength at 28 days.

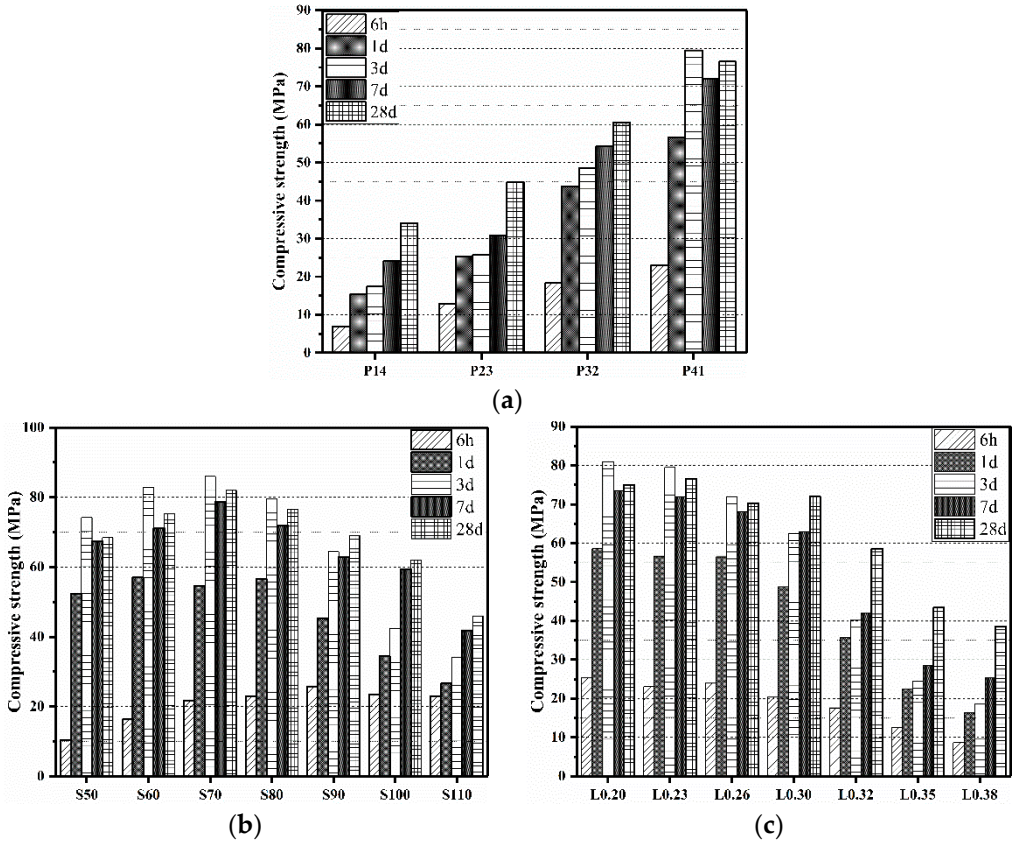

Figure 6. Effects of precursor composition, dosage of solid powdered sodium silicate and liquid–solid ratio on compressive strength: (**a**) Precursor composition, (**b**) Dosage of solid powdered sodium silicate, (**c**) Liquid–solid ratio.

It can be seen from groups P14~P41 that with the increase in the proportion of GGBS in the precursor, the compressive strength of the specimen significantly improves. The mass ratio of GGBS/fly ash in group P14 is 70/280, and the strength after 28 days is only 34.1 MPa, while the mass ratio of GGBS/fly ash in group P41 is 280/70, and the strength after 28 days reaches 76.5 MPa; this is mainly because the activity of GGBS is much higher than fly ash, and more Si and Ca are released and *C-A-S-H gel* is formed [44,45].

It can be seen from groups S50~S110 that when the dosage of powdered sodium silicate is increased from 50 to 80 g, the strength after 28 days increases slightly, which is concentrated between 70~80 MPa. When the dosage of sodium silicate is continuously increased to 110 g, the strength shows an obvious downward trend, and the 28 days strength is only 41.8 MPa. The reason for this is similar to the effect of sodium silicate content on the setting time, so it will not be repeated here.

From groups L0.20~L0.38, it can be seen that when the liquid–solid ratio increases from 0.2 to 0.3, it has no obvious effect on the compressive strength, and the strength of the test piece after 28 days is maintained above 70 MPa. When the liquid–solid ratio continues to increase to 0.38, the compressive strength decreases significantly, and the strength after 28 days is only 38.6 MPa.

3.3. X-ray Diffraction (XRD)

The XRD patterns of precursors, considering group P14, P41, S110 and L0.38 at the age of 7 days, are shown in Figure 7. It can be seen that the main product of all samples is *C-A-S-H gel* with poor crystallinity at 29.5°. The presence of the second main product, hydrotalcite, can be observed in groups P41, S110 and L0.38, where the precursor component is mainly GGBS; meanwhile, in group P14, where the precursor component is mainly fly ash, there is a lack of a hydrotalcite phase. The reason for this phenomenon is that the main components of hydrotalcite are Mg and Al in GGBS. In group P14, a large number of residual crystalline phases, including quartz, mullite and hematite, can be observed in the fly ash [46].

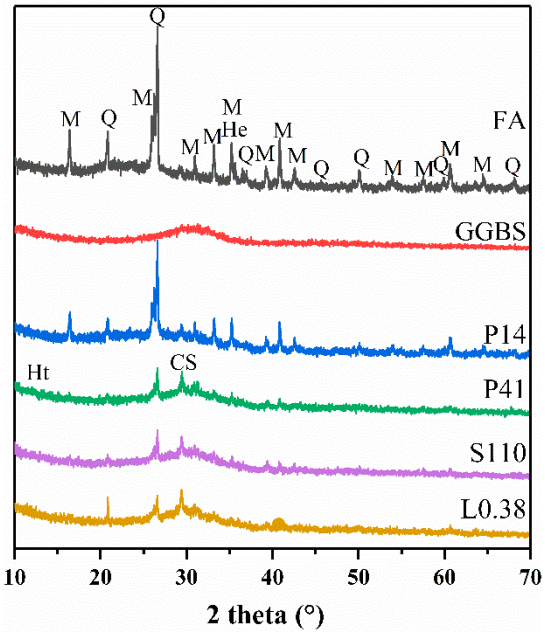

Figure 7. XRD patterns of precursors, group P14, P41, S110 and L0.38 at the age of 7 days. Legend: Q = quartz; M = mullite; He = hematite; Ht = hydrotalcite; CS = C-A-S-H.

By comparing the peak strength and position of *C-A-S-H gel* at 29.5° for each group, it can be found that although there are differences in the dosage of the alkali activator and the liquid–solid ratio among group P41, S110 and L0.38, their main product types are basically the same. The main reason for this is that their precursor components are the same, which is the most important factor affecting the gel structure [47]. Due to the different precursor components of group P14, the types of reaction products are also different. When comparing the peak of *C-A-S-H gel* in groups P41 and L0.38, group L0.38 is higher and the width is narrower, which indicates that the liquid–solid ratio improves the order degree and reaction degree of the *C-A-S-H* structure. However, since water does not participate in alkali-activated reactions, this effect is more caused by the addition of water and how it

affects the alkalinity in the system [48]. When comparing groups P41 and S110 to study the influence of the alkali activator dosage on alkali-activated reactions, it can be found that increasing the alkali activator dosage has little influence on the type and structure of the reaction products. The reasons for this are as follows [47,48]: (1) the liquid–solid ratio adopted in this paper is water/(precursor + solid alkali activator), and the addition of water is increased at the same time that the dosage of activator is increased. The results show that the concentration of Na_2O has little difference and the effect on the reaction degree is not great. (2) Since the precursor components of groups P41 and S110 are mainly GGBS, and there is sufficient Si in the system, the addition of the alkali activator-activated SiO_2 also has a very limited effect on the Al-doped *C-A-S-H gels*, and there is no change in the structure of the band.

In general, the product type and structure of alkali-activated reactions mainly depend on the mass ratio of GGBS/fly ash in the precursor; in addition, the dosage of the alkali activator and the liquid–solid ratio affect the reaction degree of the alkali-activated reaction and the number of gel products by changing the alkalinity of the system and the amount of active SiO_2 [49].

3.4. Fourier Transform Infrared Spectroscopy (FTIR)

The FTIR results of the procedures, regarding group P14, P41, S110 and L0.38, are presented in Figure 8. As can be seen from the figure, the absorption band of 691 cm^{-1} in the GGBS is related to the asymmetric tensile vibration of the tetrahedral T-O group, and its absorption is mainly at 943 cm^{-1}, which comes from the asymmetric tensile vibration of the terminal Si-O bond. The absorption band of 599 cm^{-1} in fly ash is related to the octahedral coordination aluminum in mullites, and its main absorption band is located at 1099 cm^{-1}, which corresponds to the asymmetric tensile vibration of the bridge Si-O-T bond [50].

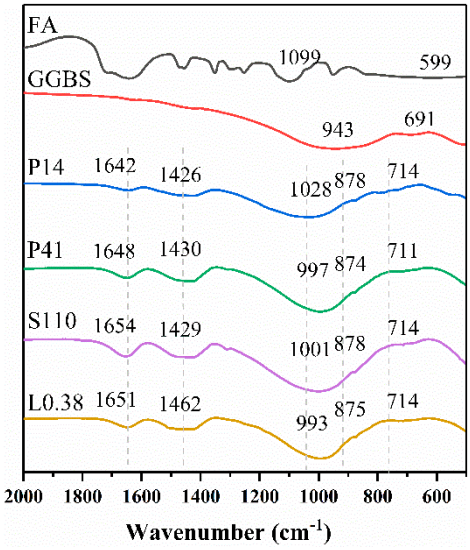

Figure 8. FTIR spectra of group P14, P41, S110 and L0.38.

In the infrared absorption spectra of all samples, absorption bands around 3400 and 1650 cm^{-1} (3400 cm^{-1} is not shown in the figure) were observed, respectively, corresponding to the bending vibration of water molecules and the a-/symmetric stretching of O-H, indicating the presence of chemically bound water in the reaction product [48]. In addition, the absorption band near 1000 cm^{-1} in each sample is the asymmetric tensile vibration of the Si-O terminal bond (non-bridging) in the reaction product, which is the representative absorption segment of the chain *C-A-S-H gel* of the product of alkali-activated GGBS, which is consistent with the diffraction peak at 29.5° in the XRD test. Compared with the absorption band of GGBS located at 943cm^{-1}, the absorption band of the Si-O terminal bond in *C-A-S-H gel* is higher, because the polymerization degree of the Si-O network in

the gel is higher; meanwhile, the absorption band of the Si-O terminal bond in the gel is lower than that of the asymmetric stretching vibration of the bridge Si-O-T bond in the fly ash [49,50]. This is because the high crosslinking bridging Si-O bond in fly ash is decomposed. It is worth noting that the gel absorption band of group P14, which is dominated by fly ash among the precursor components, is significantly higher than that of P41, S110 and L0.38, which are dominated by GGBS. This is due to the effect of Ca^{2+}. At the initial stage of the reaction, GGBS releases a large amount of Ca^{2+} in an alkali environment, which consumes the limited Si and Al units in the solution. The remaining Si and Al units are not enough to be polymerized into a high crosslinked network that is dominated by silicate and alumina (bridge Si-O bond with a high wave number), and the content of GGBS in P14 is low; therefore, the absorption band here is slightly higher than the other three groups [51]. However, when comparing P41, S110 and L0.38, it can be found that although there are differences in the dosage of the alkali activator and the liquid–solid ratio, the difference in the absorption wave number is not particularly obvious, mainly because the product *C-A-S-H gel* is limited by the chain structure, and the difference in the degree of polymerization is not large.

In addition, the absorption bands of 710, 875, and 1430 cm^{-1} were derived from O-C-O vibrations in the carbonate, possibly due to improper sample preservation and a certain degree of carbonization.

3.5. Thermogravimetry (TG/DTG)

The thermogravimetry results for group P14, P41, S110 and L0.38 are presented in Figure 9. As can be seen from the figure, all samples exhibit significant mass loss before 110 °C due to the loss of free and loosely bound water in the product. The slow mass loss at 105 °C to 300 °C is due to the dehydration decomposition of *C-A-S-H gel* [48,51]. Small DTG peaks at 300~400 °C due to the dehydration of the hydrotalcite phase, including interlayer water loss at 270 °C and main-layer dehydration at 400 °C, were not observed in P14. This is due to the low GGBS content in P14, which is consistent with the absence of the hydrous talc phase in the XRD analysis of P14 [52]. Mass loss at 600~800 °C was associated with the decomposition of calcium carbonate, and likewise, the O-C-O bond in calcium carbonate was observed in FTIR.

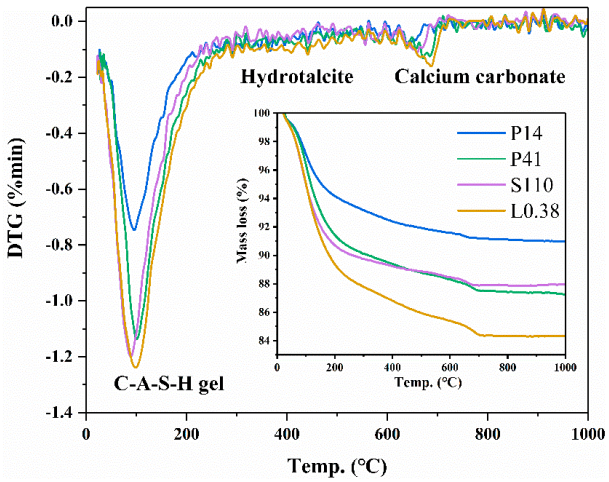

Figure 9. TG analysis of group P14, P41, S110 and L0.38.

The mass loss of each sample between 105~300 °C was observed, and the dehydration decomposition of *C-A-S-H gel* occurred mainly in this temperature range. It can be found that the mass loss of P14 was significantly lower than that of the other three groups, mainly because the content of *C-A-S-H gel* products in group P14 was less, which was explained by the lack of Ca^{2+} [47]. The mass loss of L0.38 is more than that of P41 and S110, which is consistent with the XRD analysis, demonstrating that the peak strength of group L0.38 at

29.5° is higher than that of P41 and S110. Although group L0.38 has the largest amount of *C-A-S-H gel*, its high liquid–solid ratio also leads to the matrix loosening, which leads to the poor performance of L0.38 in terms of compressive strength.

4. Conclusions

In this paper, alkali-activated GGBS/fly ash cement was prepared by mixing the precursor with solid powder sodium silicate, followed by wet mixing. The experimental results are similar to those of Nematollahi et al. [33]. When the mass ratio of GGBS/fly ash in the precursor is 1/3, the cement prepared with sodium silicate powder (Na_2SiO_3-Anhydrou activator in powder form) as the activator is about 35 MPa at 28 days. However, as the main purpose of this study was to explore the advantages and disadvantages of different types of solid sodium silicate powder, there is a lack of research on the mechanisms involved in influencing the cement performance. This paper aimed to study the influence of the mass ratio of GGBS/fly ash in the precursor, and the dosage of sodium silicate and the liquid–solid ratio on the working performance and mechanical strength of alkali-activated cement. In addition, the type, the structure and the quantity of hydration products were analyzed using XRD, TG/DTG and FTIR. The following conclusions were obtained:

1. A higher proportion of GGBS in the precursor contributes to a shorter setting time and a higher compressive strength, which also induces a decrease in the fluidity. It is recommended that the proportion of GGBS in the precursor is higher than 60%;
2. A dosage of sodium silicate within the range of 50~110 g leads to the setting time shortening, which is followed by the promotion and extension of the compressive strength promotion, and then a decline. Excessive or insufficient sodium silicate leads to the inhibition of alkali-activated reactions. On one hand, the dissolution of the precursor will be hindered; on the other hand, the formation of hydration products will be limited and there will be different optimal amounts for different precursor components. We should consider both factors in order to obtain the required cement properties;
3. The performance of alkali-activated cement can be adjusted by changing the liquid–solid ratio. Within the range of 0.20~0.38, a higher liquid–solid ratio extends the setting time and improves the fluidity of the slurry, but decreases the compressive strength;
4. The microscopic test shows that the main hydration product is *C-A-S-H gel* and that the secondary product is hydrotalcite for the mix whose precursor is mainly GGBS. The difference between them is the amount of hydration product, which can be reflected in the mass loss in TG/DTG.

Author Contributions: Methodology, Data curation, Writing—original draft, Writing—review and editing, T.D.; Funding acquisition, Supervision, T.S.; Project administration, Resources, F.X.; Data curation, G.O.; Data curation, H.W.; Data curation, F.Y.; Visualization, Z.W. All authors have read and agreed to the published version of the manuscript.

Funding: The authors gratefully acknowledge the financial support from the National Key R&D Program of China (No. 2021YFC3100805), the Third Batch of Special Fund for Science and Technology Development of Zhongshan City in 2020 (2020-18), the Sanya Yazhou Bay Science and Technology City Administration (No. SKJC-KJ-2019KY02), Shandong Province Enterprise Technology Innovation Project (202160101791), Fundamental Research Funds for the Central Universities (Nos. 2020III042 and 205259003), major science and technology project in Zhongshan city (No. 200825093739256), and China Scholarship Council, Key Research and Development Program of Hubei Province (2020BAB065), Hubei Key Laboratory of Roadway Bridge and Structure Engineering (No. DQJJ201902), the financial support from the CECSC Key Laboratory of Civil Engineering Materials-Industrial solid waste utilization (CSCEC-PT-002), Study on design and preparation of high performance concrete using Guangdong granite-based manufacture sand (CSCEC4B-2021-KTA-11), and China Scholarship Council.

Institutional Review Board Statement: Not applicable.

Informed Consent Statement: Not applicable.

Data Availability Statement: The data presented in this study are available on request from the corresponding author.

Conflicts of Interest: The authors declare no conflict of interest.

References

1. Shah, S.P.; Wang, K. Development of 'green' cement for sustainable concrete using cement kiln dust and fly ash. In Proceedings of the International Workshop on Sustainable Development and Concrete Technology, Beijing, China, 20–21 May 2004; pp. 15–23.
2. Karalar, M.; Özkılıç, Y.O.; Aksoylu, C.; Sabri, M.M.S.; Beskopylny, A.N.; Stel'Makh, S.A.; Shcherban, E.M. Flexural behavior of reinforced concrete beams using waste marble powder towards application of sustainable concrete. *Front. Mater.* **2022**, *9*, 1068791. [CrossRef]
3. Qaidi, S.; Al-Kamaki, Y.; Hakeem, I.; Dulaimi, A.F.; Özkılıç, Y.; Sabri, M.; Sergeev, V. Investigation of the physical-mechanical properties and durability of high-strength concrete with recycled PET as a partial replacement for fine aggregates. *Front. Mater.* **2023**, *10*, 1101146. [CrossRef]
4. Zeybek, Ö.; Özkılıç, Y.O.; Karalar, M.; Çelik, A.İ.; Qaidi, S.; Ahmad, J.; Burduhos-Nergis, D.P. Influence of replacing cement with waste glass on mechanical properties of concrete. *Materials* **2022**, *15*, 7513. [CrossRef]
5. Karalar, M.; Bilir, T.; Çavuşlu, M.; Özkiliç, Y.O.; Sabri, M.M.S. Use of recycled coal bottom ash in reinforced concrete beams as replacement for aggregate. *Front. Mater.* **2022**, *9*, 1064604. [CrossRef]
6. Qaidi, S.; Najm, H.M.; Abed, S.M.; Özkılıç, Y.O.; Al Dughaishi, H.; Alosta, M.; Milad, A. Concrete containing waste glass as an environmentally friendly aggregate: A review on fresh and mechanical characteristics. *Materials* **2022**, *15*, 6222. [CrossRef] [PubMed]
7. Shcherban', E.M.; Stel'makh, S.A.; Beskopylny, A.N.; Mailyan, L.R.; Meskhi, B.; Shilov, A.A.; Aksoylu, C. Normal-Weight Concrete with Improved Stress–Strain Characteristics Reinforced with Dispersed Coconut Fibers. *Appl. Sci.* **2022**, *12*, 11734. [CrossRef]
8. Beskopylny, A.N.; Shcherban', E.M.; Stel'makh, S.A.; Meskhi, B.; Shilov, A.A.; Varavka, V.; Karalar, M. Composition Component Influence on Concrete Properties with the Additive of Rubber Tree Seed Shells. *Appl. Sci.* **2022**, *12*, 11744. [CrossRef]
9. Gao, X.; Yu, Q.L.; Brouwers, H.J.H. Reaction kinetics, gel character and strength of ambient temperature cured alkali activated slag–fly ash blends. *Constr. Build. Mater.* **2015**, *80*, 105–115. [CrossRef]
10. Fan, J.; Zhu, H.; Shi, J.; Li, Z.; Yang, S. Influence of slag content on the bond strength, chloride penetration resistance, and interface phase evolution of concrete repaired with alkali activated slag/fly ash. *Constr. Build. Mater.* **2020**, *263*, 120639. [CrossRef]
11. Wei, W.D.; Wang, G. Research progress of alkali activated slag fly ash cementitious materials. In *Comprehensive Utilization of Fly Ash*; Springer: Singapore, 2008; p. 3.
12. Lee, N.K.; Lee, H.K. Setting and mechanical properties of alkali-activated fly ash/slag concrete manufactured at room temperature. *Constr. Build. Mater.* **2013**, *47*, 1201–1209. [CrossRef]
13. Li, Y.; Wu, Q.C. Study on alkali activated slag fly ash cement and concrete. *Concr. Cem. Prod.* **2000**, *5*, 42–43.
14. Song, L.X. *Study on Slag Based Polymer Pavement Repair Material*; China University of Geosciences: Wuhan, China, 2018.
15. Deng, X. *Study on Properties of Fly Ash Based Polymer for Rapid Repair of Cement Concrete Pavement*; China University of Geosciences: Wuhan, China, 2017.
16. Zhang, P.; Gao, Z.; Wang, J.; Guo, J.; Hu, S.; Ling, Y. Properties of fresh and hardened fly ash/slag based geopolymer concrete: A review. *J. Clean. Prod.* **2020**, *270*, 122389. [CrossRef]
17. Fang, G.; Ho, W.K.; Tu, W.; Zhang, M. Workability and mechanical properties of alkali-activated fly ash-slag concrete cured at ambient temperature. *Constr. Build. Mater.* **2018**, *172*, 476–487. [CrossRef]
18. Hajimohammadi, A.; Provis, J.L.; Van Deventer, J.S.J. Time-resolved and spatially-resolved infrared spectroscopic observation of seeded nucleation controlling geopolymer gel formation. *J. Colloid Interface Sci.* **2011**, *357*, 384–392. [CrossRef]
19. Matalkah, F.; Xu, L.; Wu, W.; Soroushian, P. Mechanochemical synthesis of one-part alkali aluminosilicate hydraulic cement. *Mater. Struct.* **2017**, *50*, 97. [CrossRef]
20. Adesanya, E.; Ohenoja, K.; Luukkonen, T.; Kinnunen, P.; Illikainen, M. One-part geopolymer cement from slag and pretreated paper sludge. *J. Clean. Prod.* **2018**, *185*, 168–175. [CrossRef]
21. Jizhong, L.; Qingxin, Z.; Jinrui, Z.; Sai, A. Microstructure and composition of hardening body of alkali slag-slag composite cementified material. *J. Build. Mater.* **2019**, *22*, 872–877.
22. Fenghua, J. *Study on Composition, Structure and Properties of Alkali Excited Slag Micro-Powder Cementing Materials*; Xi'an University of Architecture and Technology: Xi'an, China, 2008.
23. Koloušek, D.; Brus, J.; Urbanova, M.; Andertova, J.; Hulinsky, V.; Vorel, J. Preparation, structure and hydrothermal stability of alternative (sodium silicate-free) geopolymers. *J. Mater. Sci.* **2007**, *42*, 9267–9275. [CrossRef]
24. Hajimohammadi, A.; Provis, J.L.; Van Deventer, J.S.J. One-part geopolymer mixes from geothermal silica and sodium aluminate. *Ind. Eng. Chem. Res.* **2008**, *47*, 9396–9405. [CrossRef]
25. Hajimohammadi, A.; Provis, J.L.; Van Deventer, J.S.J. Effect of alumina release rate on the mechanism of geopolymer gel formation. *Chem. Mater.* **2010**, *22*, 5199–5208. [CrossRef]
26. Hajimohammadi, A.; Provis, J.L.; van Deventer, J.S.J. The effect of silica availability on the mechanism of geopolymerisation. *Cem. Concr. Res.* **2011**, *41*, 210–216. [CrossRef]

27. Feng, D.; Provis, J.L.; van Deventer, J.S.J. Thermal activation of albite for the synthesis of one-part mix geopolymers. *J. Am. Ceram. Soc.* **2012**, *95*, 565–572. [CrossRef]
28. Sturm, P.; Gluth, G.J.G.; Brouwers, H.J.H.; Kühne, H.C. Synthesizing one-part geopolymers from rice husk ash. *Constr. Build. Mater.* **2016**, *124*, 961–966. [CrossRef]
29. Ma, C.; Long, G.; Shi, Y.; Xie, Y. Preparation of cleaner one-part geopolymer by investigating different types of commercial sodium metasilicate in China. *J. Clean. Prod.* **2018**, *201*, 636–647. [CrossRef]
30. Mengzhu, L.; Libo, B.; Qin, W.; Shen, D. Study on mechanical properties of alkali excited slag/fly ash cementifier. *Compr. Util. Fly Ash* **2019**, *177*, 49–54.
31. Yang, K.H.; Song, J.K.; Ashour, A.F.; Lee, E.T. Properties of cementless mortars activated by sodium silicate. *Constr. Build. Mater.* **2008**, *22*, 1981–1989. [CrossRef]
32. Temuujin, J.V.; Van Riessen, A.; Williams, R. Influence of calcium compounds on the mechanical properties of fly ash geopolymer pastes. *J. Hazard. Mater.* **2009**, *167*, 82–88. [CrossRef]
33. Nematollahi, B.; Sanjayan, J.; Shaikh, F.U.A. Synthesis of heat and ambient cured one-part geopolymer mixes with different grades of sodium silicate. *Ceram. Int.* **2015**, *41*, 5696–5704. [CrossRef]
34. Yang, K.H.; Song, J.K.; Lee, J.S. Properties of alkali-activated mortar and concrete using lightweight aggregates. *Mater. Struct.* **2010**, *43*, 403–416. [CrossRef]
35. Oderji, S.Y.; Chen, B.; Ahmad, M.R.; Shah, S.F.A. Fresh and hardened properties of one-part fly ash-based geopolymer binders cured at room temperature: Effect of slag and alkali activators. *J. Clean. Prod.* **2019**, *225*, 1–10. [CrossRef]
36. Laskar, S.M.; Talukdar, S. Preparation and tests for workability, compressive and bond strength of ultra-fine slag based geopolymer as concrete repairing agent. *Constr. Build. Mater.* **2017**, *154*, 176–190. [CrossRef]
37. Nedunuri, A.S.S.S.; Muhammad, S. Fundamental understanding of the setting behaviour of the alkali activated binders based on ground granulated blast furnace slag and fly ash. *Constr. Build. Mater.* **2021**, *291*, 123243. [CrossRef]
38. Zhang, Z.; Jia, Y.; Liu, J. Influence of Different Parameters on the Performance of Alkali-Activated Slag/Fly Ash Composite System. *Materials* **2022**, *15*, 2714. [CrossRef]
39. Brough, A.R.; Atkinson, A. Sodium silicate-based, alkali-activated slag mortars: Part I. Strength, hydration and microstructure. *Cem. Concr. Res.* **2002**, *32*, 865–879. [CrossRef]
40. Song, S.; Jennings, H.M. Pore solution chemistry of alkali-activated ground granulated blast-furnace slag. *Cem. Concr. Res.* **1999**, *29*, 159–170. [CrossRef]
41. Rothstein, D.; Thomas, J.J.; Christensen, B.J.; Jennings, H.M. Solubility behavior of Ca-, S-, Al-, and Si-bearing solid phases in Portland cement pore solutions as a function of hydration time. *Cem. Concr. Res.* **2002**, *32*, 1663–1671. [CrossRef]
42. Duxson, P.; Provis, J.L.; Lukey, G.C.; Van Deventer, J.S. The role of inorganic polymer technology in the development of 'green concrete'. *Cem. Concr. Res.* **2007**, *37*, 1590–1597. [CrossRef]
43. Marjanović, N.; Komljenović, M.; Baščarević, Z.; Nikolić, V.; Petrović, R. Physical–mechanical and microstructural properties of alkali-activated fly ash–blast furnace slag blends. *Ceram. Int.* **2015**, *41*, 1421–1435. [CrossRef]
44. Duxson, P.; Fernández-Jiménez, A.; Provis, J.L.; Lukey, G.C.; Palomo, A.; van Deventer, J.S. Geopolymer technology: The current state of the art. *J. Mater. Sci.* **2007**, *42*, 2917–2933. [CrossRef]
45. Fernández-Jimenez, A.; De La Torre, A.G.; Palomo, A.; López-Olmo, G.; Alonso, M.M.; Aranda, M.A.G. Quantitative determination of phases in the alkali activation of fly ash. Part I. Potential ash reactivity. *Fuel* **2006**, *85*, 625–634. [CrossRef]
46. Tran, V.A.; Nguyen, H.A. Evaluation on comprehensive properties and bonding performance of practical slag-fly ash blending based alkali-activated material. *J. Build. Eng.* **2022**, *62*, 105350. [CrossRef]
47. Gao, X.; Yu, Q.L.; Brouwers, H.J.H. Properties of alkali activated slag–fly ash blends with limestone addition. *Cem. Concr. Compos.* **2015**, *59*, 119–128. [CrossRef]
48. Zhang, S.; Keulen, A.; Arbi, K.; Ye, G. Waste glass as partial mineral precursor in alkali-activated slag/fly ash system. *Cem. Concr. Res.* **2017**, *102*, 29–40. [CrossRef]
49. Gao, X.; Yu, Q.L.; Brouwers, H.J.H. Characterization of alkali activated slag–fly ash blends containing nano-silica. *Constr. Build. Mater.* **2015**, *98*, 397–406. [CrossRef]
50. Labbez, C.; Pochard, I.; Jönsson, B.; Nonat, A. CSH/solution interface: Experimental and Monte Carlo studies. *Cem. Concr. Res.* **2011**, *41*, 161–168. [CrossRef]
51. Zhang, S.; Li, Z.; Ghiassi, B.; Yin, S.; Ye, G. Fracture properties and microstructure formation of hardened alkali-activated slag/fly ash pastes. *Cem. Concr. Res.* **2021**, *144*, 106447. [CrossRef]
52. Zhang, J.; Shi, C.; Zhang, Z. Effect of Na_2O concentration and water/binder ratio on carbonation of alkali-activated slag/fly ash cements. *Constr. Build. Mater.* **2021**, *269*, 121258. [CrossRef]